Nonlinear Aeroelastic Responses of an Airfoil with a Control Surface by Precise Integration Method

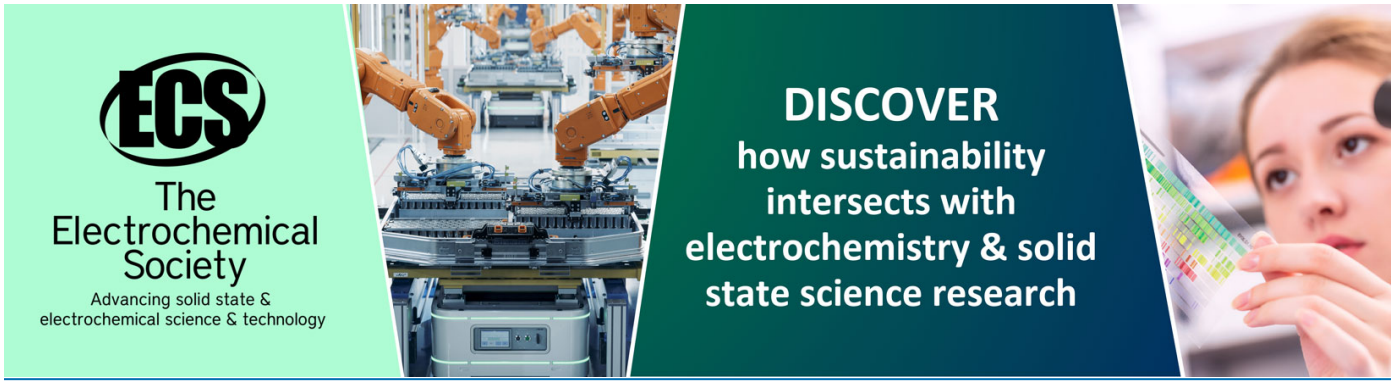

Nonlinear Aeroelastic Responses of an Airfoil with a Control Surface by Precise Integration Method

Xiwen Huang[1], Suxin Xie[2], Yunping Zhang[3] and Yanmao Chen[1,*]

[1]Department of Mechanics Sun Yat-sen University, Guangzhou 510275, China
[2]Basic Course Teaching Department Jiangxi Industry Polytechnic College Nanchang 330039, China
[3]Nari Technology Development Limited Company, 20 High-Tech Road, Nanjing 210061, China

*Corresponding author

Abstract. This paper presents a highly accurate algorithm, based on precise integration method (PIM), to investigate the aeroelastic system of an airfoil with control surface. The nonlinear system is separated as linear sub-systems, which are solved by PIM stepwise. During each step, a predictor-corrector algorithm is proposed to detect switching points between sub-systems. Numerical examples show that, the presented algorithm is much more accurate and efficient than the widely-used Runge-Kutta method. Sometimes, the Runge-Kutta method even provides false results. With such high precision and efficiency, the presented algorithm has the potential to become a benchmark for comparison in solving piecewise-smooth dynamical systems.
Keywords: Airfoil; Control surface; Piecewise; Aeroelastic; Precise integration method.

1. Introduction

In most cases, there is no analytical solution for nonlinear aeroelastic systems, or at least the analytical solution is not evident. For this reason, it is rare to find contributions made to seek an analytical solution. Alternatively, a large amount of research works were presented to predict the non-decaying aeroelastic responses of an airfoil via semi-analytical or numerical solution techniques [1]. Many semi-analytical methods based more or less on harmonic balancing were proposed, such as the harmonic balance method [2], the fast harmonic balance technique [3], the incremental harmonic balance method [4] and the homotopy analysis method [5], to mention a few.

Mathematically, it is usually not easy to implement semi-analytical solution procedures though they exhibit some merits over numerical simulations. To date, semi-analytical approaches have been mainly employed in analyzing low-dimensional aeroelastic systems with simple nonlinearities such as cubic stiffnesses. It is necessary to develop effective numerical methods to solve aeroelastic systems with high dimensions and/or subjected to complicated nonlinearities such as freeplay or hysteresis. In fact, many numerical techniques are capable of solving these complex systems, for example, the Runge-Kutta (RK) method [6,7], the differential transformation method [8], the point transformation method [9], the perturbation-incremental method [10], and a newly initiated multiple scale time domain collocation method [11]. Among them, the RK is probably the most widely implemented method. To some extent, it has been a benchmark for comparison of numerical as well as semi-analytical approaches [12,13].

As mentioned above, effective solution procedures of long-term responses such as limit cycle oscillations (LCOs) and chaotic responses play a pivotal role in the investigations of aeroelastic

systems. It is usually cumbersome, however, to obtain reliable long-term numerical solutions for nonlinear systems [14,15]. As non-smooth nonlinearities are included, it can become even tougher. More specifically, a computational obstacle will be confronted in determining switching points resulted from piecewise nonlinearities [16]. The piecewise stiffness, as one of typical non-smooth nonlinearities, usually results from loose hinges of external stores or control surfaces. Lin and Cheng [17] reported that, an entirely incorrect asymptotic behavior can occur due to the accumulative error in tracking the state response happening exactly at switching points.

To tackle this problem, a simple yet efficient algorithm has been proposed to solve the airfoil aeroelastic system with either a freeplay [18,19] or an external store [20]. This algorithm is based on the precise integration method (PIM) initiated by Zhong et al [21] two decades ago. The outstanding merits of the PIM lie in its high precision and computation efficiency [22]. It is necessary and worthwhile to further extending the presented algorithm, so that it can solve both steady and transient responses over the whole solution domain. As there are neither non-autonomous nor external forcing terms, the considered system can be transformed into a homogeneous one. It is therefore very simple to carry out the PIM procedures. More importantly, both the high precision and efficiency of the PIM can be maintained with the help of a predictor-corrector process.

2. Equations of Motions

The typical airfoil section with a control surface as three degrees-of-freedom denoted by a plunge displacement *h,* positive in the downward direction, a pitch angle α and a control surface angle β, both positive in the nose up, as shown in Ref. [23]. The semi-chord length of the airfoil section is denoted as *b*. The elastic axis is located at a distance *ab* from themid-chord with *a* as a non-dimensional coefficient. The mass center (c.g.) of the wing is located at a distance $x_\alpha b$ from the elastic axis. Both the two distances are positive when measured towards the airfoil trailing edge. There is a distance *cb* from the hinge line of the control surface, and a distance $x_\beta b$ from the mass center of the control surface to the mid-chord. The motions of the airfoil can be described by the following equations [23]

$$
\begin{aligned}
r_\alpha{}^2\ddot{\alpha} + \left[r_\beta{}^2 + (c-a)x_\beta\right]\ddot{\beta} + x_\alpha\ddot{h} + 2m_\alpha\omega_\alpha\varsigma_\alpha\dot{\alpha} + r_\alpha{}^2\omega_\alpha{}^2\alpha &= M_\alpha/(mb^2)\\
\left[r_\beta{}^2 + (c-a)x_\beta\right]\ddot{\alpha} + r_\beta{}^2\ddot{\beta} + 2m_\beta\omega_\beta\varsigma_\beta\dot{\beta} + r_\beta{}^2\omega_\beta{}^2G(\beta) &= M_\beta/(mb^2)\\
x_\alpha\ddot{\alpha} + x_\beta\ddot{\beta} + (m_t/m)\ddot{h} + 2m_h\omega_h\varsigma_h\dot{h} + \omega_h{}^2h &= L/(mb).
\end{aligned}
\tag{1}
$$

where the dot denotes the differentiation with respect to the non-dimensional time defined as $t=Ut_1/b$ with t_1 as the real time (second) and *U* as the flow speed (m/s), *m* represents the modal mass per unit span for each degree of freedom, m_t is the total mass of the modal per unit span, ω is the uncoupled natural frequency, ς is the measured damping ratio, r_α is the radius of gyration about the wing-aileron, r_β is the reduced radius of gyration of aileron, *L* denotes the aerodynamic lift, and M_α, M_β represent the aerodynamic moment of wing-aileron and aileron, respectively. The model stiffnesses are normalized by $K_\alpha = m_\alpha\omega_\alpha^2$, $K_\beta = m_\beta\omega_\beta^2$ and $K_h = m_h\omega_h^2$. The unsteady aerodynamic force and moments in incompressible flow are as follows [23]

$$
\begin{aligned}
M_\alpha = -\rho b^2\{\pi\left(\tfrac{1}{2-a}\right)Ub\dot{\alpha} + \pi b^2\left(\tfrac{1}{8+a^2}\right)\ddot{\alpha} + (T_4+T_{10})U^2\beta + (T_1 - T_8 - (c-a)T_4 +\\
(1/2)T_{11})Ub\dot{\beta} - [T_7 + (c-a)T_1]b^2\ddot{\beta} - a\pi b\ddot{h}\} + 2\rho Ub^2\pi\left(\tfrac{a+1}{2}\right)C(k)(U\alpha + \dot{h} + b\left(\tfrac{1}{2-a}\right)\dot{\alpha} +\\
1/\pi\, T_{10}U\beta + b(1/2\pi)T_{11}\dot{\beta}).
\end{aligned}
\tag{2}
$$

$$
\begin{aligned}
M_\beta = -\rho b^2\{\left(-2T_9 - T_1 + T_4\left(\tfrac{a-1}{2}\right)\right)Ub\dot{\alpha} + 2T_{13}b^2\ddot{\alpha} + \left(\tfrac{1}{\pi}\right)U^2\beta(T_5 - T_4T_{10}) -\\
(1/2\pi)Ub\dot{\beta}T_4T_{11} - \left(\tfrac{1}{\pi}\right)T_3b^2\ddot{\beta} - T_1\mathrm{b}\ddot{h}\} \times \rho Ub^2T_{12}C(k)(U\alpha + \dot{h} + b\left(\tfrac{1}{2-a}\right)\dot{\alpha} + 1/\pi\, T_{10}U\beta +\\
b\left(\tfrac{1}{2\pi}\right)T_{11}\dot{\beta}.
\end{aligned}
\tag{3}
$$

$$L = -\rho b^2\left(U\pi\dot{\alpha} + \pi\ddot{h} - \pi ba\ddot{\alpha} - UT_4\dot{\beta} - T_1 b\beta\right) - 2\pi\rho UbC(k)\left(U\alpha + \dot{h} + b\left(\frac{1}{2-a}\right)\dot{\alpha} + 1/\pi T_{10}U\beta + b\left(\frac{1}{2\pi}\right)T_{11}\dot{\beta}\right). \quad (4)$$

The Theodorsen constants $T_i(i = 1,2,\ldots,\ 8)$ are referred to [23]. And, the loading associated with the Theodorsen's function $C(k)f(t)$ is represented by the Duhamel formulation in the time domain. More details of the generalized Theodorsen function $C(k)$ can be found in Ref. [24].

$$L_c = C(k)f(t) = f(0)\phi(t) + \int_0^t \frac{\partial f(\sigma)}{\partial\sigma}\phi(t-\sigma)d\sigma. \quad (5)$$

where

$$f(t) = U\alpha + \dot{h} + b\left(\frac{1}{2-a}\right)\dot{\alpha} + 1/\pi\, T_{10}U\beta + b\frac{1}{2\pi}T_{11}\dot{\beta}. \quad (6)$$

and $\phi(t)$ is the Wagner function. In order to simplify the convolution terms, the Sear's approximation [23]

$$\phi(t) \approx c_0 - c_1 e^{-c_2 t} - c_3 e^{-c_4 t}. \quad (7)$$

can be employed with $c_1 = 0.165, c_2 = 0.0455, c_3 = 0.335$, and $c_4 = 0.3$.
The final step in simplifying the Theodorsen function is to represent the integral term using the inverse Laplace transformation. After two augmented variables are introduced as $x_{a1} = y,\ x_{a2} = \dot{y}$, the coupled state space system given by Eq. (1) can be rewritten as a set of eight first-order ordinary differential equations as

$$\dot{X} = AX + B. \quad (8)$$

where $X = [\alpha\ \ \beta\ \ \frac{h}{b}\dot{\alpha}\dot{\beta}\frac{\dot{h}}{b}x_{a1}x_{a2}\ ]^T$, matrix A and vector B are both given in Ref. [23].
For a freeplay nonlinearity due to the looseness of the control surface, the control surface moment takes the form as

$$G(\beta) = \begin{cases} \beta - \delta, & \beta > \delta \\ 0, & -\delta \le \beta \le \delta \\ \beta + \delta, & \beta < -\delta \end{cases}. \quad (9)$$

where δ is the beginning of the freeplay.

3. The PIM with a Predictor-corrector Procedure

As the freeplay is included, system (8) becomes non-smooth and can be decomposed into three sub-systems in a vector form as

$$\dot{X} = A_i X + B_i. \quad (10)$$

with A_i and B_i as the respective coefficient matrixes for sub-system i (i=1,2 and 3). The expressions for these matrixes are given in Ref. [25]. We can transform (10) into homogeneous equations, since the coefficient matrixes (A_i) are all reversible. Introducing the transformation $Y = X + A_i^{-1}B_i$, we have

$$\dot{Y} = A_i Y \quad (11)$$

By this means, the PIM can be employed to solve homogeneous equations (i.e., (11)) rather than inhomogeneous ones (i.e., (10)). By this means, the state X can also be obtained according to the inverse transformation, i.e., $X = Y - A_i^{-1}B_i$. For each sub-system in (11), its general solution is

$$Y = \exp(A_i t)Y(0). \quad (12)$$

with $Y(0)$ as an IC defined as $Y(0) = X(0) + A_i^{-1}B_i$. Given a time series [0, Δt,2Δt, …, $N\Delta t$] with Δt as one time step and N as the number of integration steps, the state solution at the nth time point can be described as

$$Y^n = T^n Y(0) \tag{13}$$

with T=exp($A_i\Delta t$) as the exponential matrix for each time step. More details for the computation of the exponential matrix are referred to Zhong [21].

If the second component of X, i.e., β, never passes either one of the two switching points (-δ or δ), the whole time histories can be accurately generated during one of the linear sub-systems. In most cases, however, the state switches from one sub-system to another as β passes any one of the switching points.

Denote μ as the switching value, and introduce a ratio $\lambda = (\mu - \beta^n)/(\beta^{n+1} - \beta^n)$. We predict that the time needed for X^n to approach the switching value is about $\lambda\Delta t$. Hence, the predicted state can be corrected as $Y^{n+1} = Y^n \exp(A_i\lambda\Delta t) = T^\lambda Y^n$. Then we can calculate $X^{n+1} = Y^{n+1} - A_i^{-1}B_i$. Note that, the ratio is equal to 1 if X^{n+1} is exactly located at the switching point, that means, $\beta^{n+1} = \mu$. The predictor-corrector algorithm is to repeat (14) and (15) until λ approaches 1 closely enough.

4. Numerical Results and Discussions

The system parameters are given as follows [23] $b = 0.127$ m, $a = -0.5$, $c = 0.5$, $m = 1.558$ kg/m, $m_t = 1.2895$ kg, $r_\alpha = 0.7321$, $r_\beta = 0.11397$, $x_\alpha = 0.434$, $x_\beta = 0.019$, $k_\alpha = 14861\ \mathrm{s}^{-2}$, $k_\beta = 1551\ \mathrm{s}^{-2}$, $k_h = 18091\ \mathrm{s}^{-2}$, $\varsigma_\alpha = 0.01626$, $\varsigma_\beta = 0.0115$, $\varsigma_h = 0.0113$, $\rho = 1.225$ kg/m^2, $\delta = 0.349$ and the value of U varies. Figure 1 shows the phase planes for LCOs with U=49 obtained by PIM and by RK, respectively. Clearly, excellent consistence can be observed between these results.

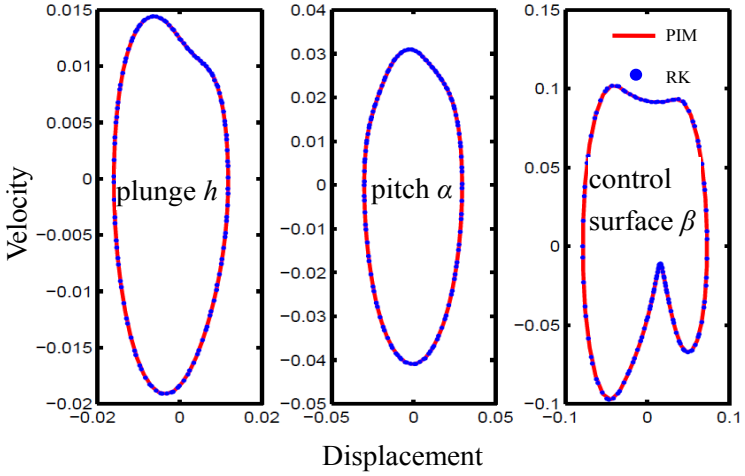

Figure 1. The phase planes of LCOs obtained by PIM and RK with U=49, respectively.

In order to further examine the accuracy of the presented method, we calculate the norm ||X-X_e||, here X is the PIM or RK result and X_e denotes the exact solution. Note that, the exact solution is obtained stepwise by repeatedly applying the theories of ordinary differential equations as the state switches from one sub-system to another. Note that, a severe computational obstacle will be resulted from determining the states at switching points by a tedious binary searching strategy. The logarithmic errors of the respective solutions provided by PIM and RK compared with the exact ones are illustrated in Fig. 2. The PIM error is at the order of magnitude about 10^{-10} or so. More importantly, the computation accuracy can maintain to be high level regardless of the time step. According to Zhong [21], the accuracy can even reach the computer accuracy in principle. Specifically, the accuracy of the presented algorithm can be further improved as the tolerance error is refined in the predictor-corrector algorithm. As for the RK method, the corresponding errors are about 10^{-4} and 10^{-6} for Δt as 0.1 and 0.01, respectively. It is reasonable to say the PIM has much higher computation

precision than RK.

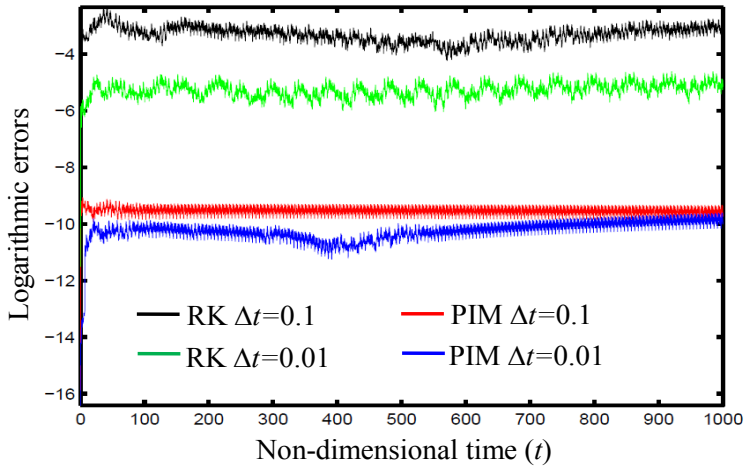

Figure 2. Logarithmic errors of RK or PIM results versus the exact solutions of the aeroelastic system with U=49.

Note that, the exact solutions are obtained by solving the sub-systems step by step according to the theories of ordinary differential equations. The computation is dramatically expensive, since a set of 10 ordinary differential equations have to be solved repeatedly as the state vector (X) switches between the three sub-systems. The CPU running time spent on getting either the RK or exact solution is much longer than that used in PIM, as shown in Fig. 3. As discussed above, the PIM error does not increase significantly as the step length is chosen much longer. By lengthening the time step in PIM, therefore, the computational efficiency can be even improved without losing substantial precision. As for RK, usually, the accuracy has to be improved by shortening the time step, which is at the expense of dramatically increasing computational resources. It is reasonable to say, therefore, the presented algorithm is indeed suitable for long-term simulation.

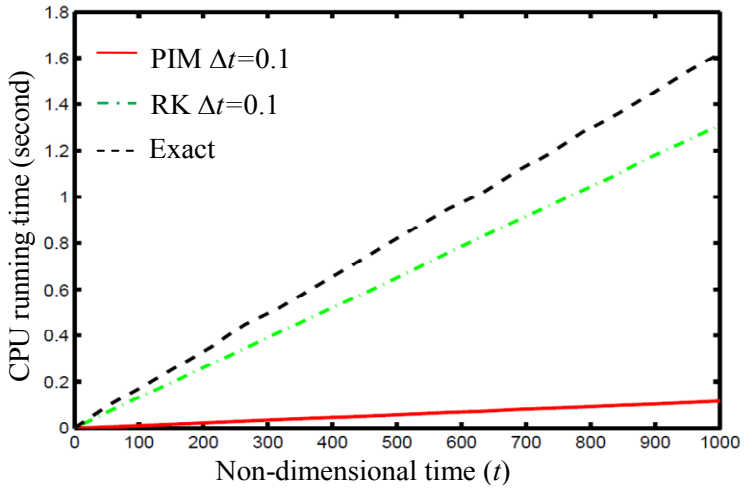

Figure 3. The CPU running time of RK, PIM and exact solution spent on solving the aeroelastic system with U=49.

5. Conclusion

A highly accurate algorithm has been proposed to solve the aeroelastic system of an airfoil section with a control surface. The presented algorithm is based on the precise integration method and a predictor-corrector scheme. Numerical examples show that the results can be obtained accurately and efficiently by the presented algorithm, when compared with the exact solutions and the widely-used RK method. Moreover, the precision remains to be at the same order of magnitude regardless of the step length. This is an outstanding merit of the presented algorithm over some other time-stepping

integration methods. One can get the dynamic responses more efficiently in any desired long-term duration by lengthening the time step without losing substantial precision.

Acknowledgement
This work is supported by the National Natural Science Foundation of China (11572356, 11672337).

References

[1] E.H.Dowell, D.Tang, Nonlinear aeroelasticity and unsteady aerodynamics, AIAA J. 40 (2002) 1697-1707.
[2] Y.M.Chen, J.K.Liu, On the limit cycles of aeroelastic systems with quadratic nonlinearities, Struct. Eng. Mech. 30 (1) (2008) 67-76.
[3] H.H.Dai, X.K.Yue, J.P.Yuan, and D. Xie, A fast harmonic balance technique for periodic oscillations of an aeroelastic airfoil, J. Fluid. Struct. 50 (2014) 231-252.
[4] J.K.Liu, F.X.Chen, Y.M.Chen, Bifurcation analysis of aeroelastic systems with hysteresis by incremental harmonic balance method, Appl. Math. Comput. 219 (2012) 2398-2411.
[5] Y.M.Chen, J.K.Liu, Homotopy analysis method for limit cycle flutter of airfoils, Appl. Math. Comput. 203 (2008) 854-63.
[6] Jorge álvarez, Jesús Rojo, An improved class of generalized Runge–Kutta methods for stiff problems. Part I: The scalar case, Appl. Math. Comput. 130 (2002) 537-560.
[7] B.H.K.Lee, S.J.Price, Y.S.Wong, Nonlinear aeroelastic analysis of airfoils: bifurcation and chaos, Prog. Aerosp. Sci. 35 (1999) 205-344.
[8] C.C.Wang, C.L.Chen, H.T.Yau, Bifurcation and chaotic analysis of aeroelastic systems, J. Comput. Nonlinear Dyn. 9 (2014) 021004.
[9] L.Liu, Y.S.Wong, B.H.K.Lee, Nonlinear aeroelastic analysis using the point transformation method, Part 1: freeplay model, J. Sound Vib. 253 (2002) 447-469.
[10] K.W.Chung, C.L.Chan, B.H.K.Lee, Bifurcation analysis of a two-degree-of-freedom aeroelastic system with freeplay structural nonlinearity by a perturbation- incremental method, J. Sound Vib. 299 (2007) 520-39.
[11] H.H.Dai, X.K.Yue, C.S. Liu, A multiple scale time domain collocation method for solving non-linear dynamical system, Int. J. Non-linear Mech. 67 (2014) 342-351.
[12] H.H.Dai, X.K.Yue, D.Xie, S.N. Atluri, Chaos and chaotic transients in an aeroelastic system, J. Sound Vib. 333 (2014) 7267-7285.
[13] S.A.Fazelzadeh, A.Mazidi, Nonlinear aeroelastic analysis of bending-torsion wings subjected to a transverse follower force, J. Comput. Nonlinear Dyn. 6 (2011) 031016.
[14] S.J.Liao, P.F. Wang, On the mathematically reliable long-term simulation of chaotic solutions of Lorenz equation in the interval [0,10000], Sci. China, Phys., Mech. Astronomy. 57 (2014) 330-335.
[15] H.J.Wang, C.W.Shu, Q.Zhang, Stability analysis and error estimates of local discontinuous Galerkin methods with implicit-explicit time-marching for nonlinear convection-diffusion problems, Appl. Math. Comput. 272 (2016) 237-258.
[16] D.D.Bueno, L.C.Sandoval Góes, P.J.P. Gonçalves, Control of limit cycle oscillation in a three degrees of freedom airfoil section using fuzzy Takagi-Sugeno modeling, Shock Vib. (2014) 597827.
[17] W.B.Lin, W.H. Cheng, Nonlinear flutter of loaded lifting surfaces, J. Chin. Soc. Mech. Eng. 14 (1993) 446-466.
[18] C.C.Cui, J.K.Liu, Y.M.Chen, Simulating nonlinear aeroelastic responses of an airfoil with freeplay based on precise integration method, Commun. Nonlinear Sci. Numer. Simulat. 22 (2015) 933-942.
[19] W.Tian, Z.Yang, Y. Gu, Dynamic analysis of an aeroelastic airfoil with freeplay nonlinearity by precise integration method based on Padé approximation, Nonlinear Dyn. 89 (2017) 2173-2194.
[20] Y.M.Chen, J.K.Liu, Nonlinear aeroelastic analysis of an airfoil-store system with a freeplay by precise integration method, J. Fluid. Struct. 46 (2014) 149-164.

[21] W.X.Zhong, F.W. Williams, A precise time step integration method, Proceeding Institution Mech. Eng. 208 (1994) 427-430.
[22] W.X.Zhong, On precise integration method, J. Comput. Appl. Math. 163 (2004) 59-78.
[23] L.P. Liu, E.H. Dowell, Harmonic balance approach for an airfoil with a freeplay control surface, AIAA J. 43 (2005) 802-815.
[24] T.Theodorsen, General Theory of Aerodynamic Instability and the Mechanism of Flutter, NACA Rept. 496. (1935)
[25] R.Vasconcellos, A.Abdelkefi, F.D.Marques, and M.R.Hajj, Representation and analysis of control surface freeplay nonlinearity, Journal of Fluids and Structures. 31 (2012) 79-91.